Three-dimensional Simulation of the Field Patterns Generated by an Integrated Antenna

Jonathan Blackledge and Bazar Babajanov*

Abstract— **Simulating the electromagnetic field patterns generated by integrated antennas used in mobile phones, for example, is fundamental to understanding their transmission characteristics and thereby engineering designs that optimise the directional properties of electromagnetic propagation. Modern integrated antennas have complex three-dimensional geometry designed to optimise their performance in terms of their multi-band and multi-modal attributes. This geometry, coupled with their close proximity to other component of the device (such as the battery and Printed Circuit Board, for example) produce complex field patterns due to the scattering of the electric (and magnetic) field within a spatial domain that is the same order of scale as the wavelength. Simulating this interaction therefore requires models that are generalised and not specific to an idealised antenna geometry. In this paper we present a three-dimensional model for simulating the interaction of an electromagnetic field generated by antennas whose geometry is arbitrary with complex dielectric components in the near-field, in particular, the Fresnel zone. The resulting field pattern is then taken to be a secondary source, whose far-field intensity map is computed by application of a Fourier transform. The material properties of the dielectric are taken to include variations in the relative permittivity and conductivity which are assumed to be isotropic. The evaluation of the scattered electromagnetic field is undertaken using a new approach based on a free space Green's function to the Poisson equation whose properties are compared to the conventional Green's function solution to the inhomogeneous Helmholtz equation. Some example simulations are provided to illustrate the approach used which include fractal antennas based on self-similar patterns.**

Keywords: Microwave propagation, near-field interaction, far-field radiation pattern, integrated antennas.

1 Introduction

Modern mobile phones and other mobile devices have a range of emission/reception components which include GSM (Global System for Mobile communications), 3G (3rd Generation of mobile telecommunications technology), LTE (Long Term Evolution, marketed as 4G LTE and a standard for wireless communication of high-speed data for mobile phones and data terminals), Bluetooth (a wireless technology standard for exchanging data over short distances), WLAN (Wireless Local Area Network), GPS (Global Positioning System). DVB-H (Digital Video Broadcasting - Handheld) and FM (for FM radio reception). This requires advances in mobile technology to increase their portfolio of reception and/or transmission/reception features which, in turn, requires a range of integrated antennas for operation over a broad range of frequencies. For example, the standard iPhone has four antennas for Bluetooth, Wi-Fi, GPS, UMTS and GSM. In this context there has and continues to be advances in the development of models, simulators and processes whose purpose is to enhance the design of antennas and their integration and embedding into portable units [1], [2] for the optimisation of mobile communications [3]. This includes, for example, multi-beam directional antennas [4] and the development of smart antennas [5] for both narrow band and ultra-wide-band systems [6].

The principal requirements that 'drive' the development of mobile phones are the reduction in physical size and weight, low cost, high efficiency and low SAR levels, i.e. the Specific Absorption Rate (SAR) which is a measure of the rate at which energy is absorbed by the body when exposed to a radio frequency electromagnetic field. With regard to service providers and the development of a cellular network infrastructure, the primary issues concern the provision of a multi-band capability and broadband operations which are robust to environmental changes while optimising the use of channel capacity. In terms of electromagnetic field configuration, the challenge is

*Jonathan Blackledge (jonathan.blackledge@dit.ie) is the Science Foundation Ireland Stokes Professor at Dublin Institute of Technology (DIT) and Director of the Information and Communications Security Research Group. Bazar Babajanov (a.murod@mail.ru) is Assistant Professor at the Department of Mathematical Physics, Urgench State University, Uzbekistan

to design small antennas which are internal to the mobile device, are light weight and cheap to mass produce, are multi-band and incorporate integrated multi-antenna systems. Since the early 1990s there has been a general decrease in the size, weight and price of a mobile phone while the functionality and performance has increased significantly morphing into the era of the smart phone from 2008 to date. An important component of this development has been the design of high frequency radio antennas which include the use of patch antennas instead of whips, ergonomic issues such as tapering and weighting to encourage users to hold the device below the antenna and the use of plastic casings. The first GSM-phone with an integrated antenna was the Hagenuk Global Handy launched in 1996 which pioneered the use of increasingly sophisticated integrated multi-band antennas that are common today. The principal advantage of developing integrated (as opposed to external) antennas is aesthetics, low cost and robustness but this comes at the price of the small available volume, shadowing and the interaction with other components. This paper focuses on modelling this interaction.

The development of all mobile phones can be considered to involve three principal components, the chargeable battery, the integrated electronics (including software) and the integrated antenna. With regard to the latter two categories, there is a clear distinction that can be considered: wheres Moore's law (i.e. the number of transistors that can be placed inexpensively on an integrated circuit doubles approximately every two years) can loosely be applied to the evolution of the electronic sophistication of a mobile phone, the antennas can ultimate only follow Maxwell's law (i.e. the properties of electromagnetic fields as defined by Maxwell's equations). Thus, the simulation of antenna performance using products such as *Feko* [7], *EMWorks* [8] and *CST* [9], for example, is critical to the antenna design which is coupled with its mechanical design, measurement of the electromagnetic field intensity patterns, prototyping and production in terms of the available space, shape and pre-defined position of feed contacts. In this context, typical design concept for a mobile phone include bar phones with integrated antennas, flip-phones with an external antenna, bar phones with helical antennas and slide phone with an integrated antenna.

One of the limiting factors associated with any antenna design is the Chu-Harrington bandwidth limit [10], [11] which sets a lower limit on the Q (Quality) factor for a small radio antenna. The Q factor is a dimensionless parameter that characterises a resonator's bandwidth $\Delta\omega$ relative to its carrier frequency ω_0 (where ω is the angular frequency) and is given by

$$Q = \frac{\omega_0}{\Delta\omega}$$

The maximum bandwidth is therefore determined by the minimum Q. For an antenna in free space enclosed in a sphere of radius a the minimum Q factor is given by

$$Q_{\min} = \frac{1 + 3k^2a^2}{k^3a^3(1 + k^2a^2)})$$

a relationship that implies that there is a compromise required between the enclosing volume of the antenna and the available bandwidth. Optimising this relationship is therefore an important issue in mobile antenna development. Other factors include the effect of a finite ground plane, handset components such as the battery and the user's presence. Referring to Figure 1 [12] which shows the basic geometry for a Planar Inverted F-Antenna (PIFA), in order to generate a resonator we need to incorporate the condition (for wavelength λ)

$$L + H \sim \frac{\lambda}{4}$$

which requires miniaturisation of a folded radiator. Further the input impedance is a function of S and the bandwidth is a function of H and W. This requires that the shape of the antenna is adapted to the phone cover and that slots and cuts are introduce into the radiator to generate multi-modality. If a patch antenna of the type illustrated in Figure 1 is mounted of the PCB (Printed Circuit Board) then the current distribution on the patch induces currents on the PCB which are frequency related. In turn, this can contribute to the electromagnetic field that is generated. This effect, coupled with the geometry of the antenna and the context of its integrated design requires simulation of the expected Electromagnetic (EM) radiation pattern. There are a range of EM field simulators available for this purpose but they all have limitations associated with the geometry (including size, structure and complexity), the physical and mathematical model (in terms of the limiting conditions imposed such as the isotropy and absorbing properties of the materials) and computational effects such the use of irregular grids and spatial truncation. The resolution of the grid upon which the simulation is undertaken also incurs computational costs especially when a fully three-dimensional simulator is being considered. The simplest simulator is to consider the radiation field pattern in the far-field to be given by the Fourier transform of the antenna geometry (the source function). Simulation of the field pattern in the near-field involves convolution with the free space Green's function and in the intermediate zone, convolution with a Fresnel Point Spread Function. However,

simulations of this type, irrespective of there sophistication in terms of a GUI and graphical representations, do not usually take into account the interaction (scattering) of the field emitted by the antenna with near-field structures associated with an integrated design.

In this paper, we consider a fully three dimensional Voxel based model whose principal aim is to provide a far-field simulation of the radiative field generated by the near-field scattering effects associated with an integrated multi-model antenna. After providing a brief overview of the issues associated with cellular antennas in Section II, Section III introduces the electromagnetic model starting from Maxwell's equations and derives the inhomogeneous wave equation whose solution is required and considers the principal conditions associated with the derivation. Section IV investigates the solution used to evaluate the three-dimension electric wavefield pattern in the Fresnel and Fourier zones. This is achieved using a conventional free space Green's function method but using a non-conventional approach to obtaining a series solution for the scattered field. The solution obtained is used in Section V to introduce the principal steps associated with the simulation for a simplified source-reflector system. Finally, in Section VI, we consider the simulation of radiation field patterns focusing on, by way of an example, fractal antennas which have properties that are ideally suited for operations over a range of frequencies. This includes the computation of the current density induced by the back-scattered electric field.

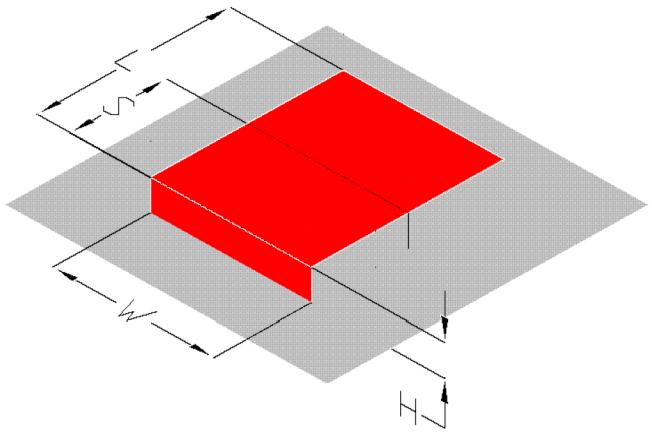

Figure 1: Basic geometry of a PIFA internal antenna which is a simplified schematic of antennas with more complex topologies used for 3G and GSM reception. Source:[12]

2 Cellular Antennas

An antenna without gain (0 dB) radiates an electromagnetic wavefield in all directions equally whereas antennas with gain redirects or concentrates electromagnetic energy in a certain direction, the gain in performance being measured in the direction of the energy concentration. In both cases, the spatial distribution of the electromagnetic energy can be characterised by computing the square modulus of the (complex) wavefield once it has been measured experimentally and/or simulated numerically. The models used to simulate such fields fall into two distinct classes: near-field modelling where the wavefield is analysed within a few wavelengths of the source and far-field modelling in which the wavefield is analysed many wavelengths away from the source. The purpose of modelling the field pattern generated from an integrated antenna is to assess the directional properties subject to a given design.

In simple terms, a low gain cellular antenna performs better in areas where the signal is subject to multiple reflections that occur in urban areas, for example, and is generally oriented vertically with regard to the antenna mast. A vertically mounted high gain antenna directs more energy parallel to the earth and less energy toward the sky. These antennas perform best when the mast is unobstructed and located on the horizon (e.g. oceans, lakes, deserts). For users who travel to remote areas of poor cellular signal and varying geographic terrain, both types of antennas are required because of this phenomenon.

In the frequencies ranges used for cellular mobile communications, 0 dB gain or quarter wave antennas are relatively short and usually on the cm scale. The length of antennas used in different types of communication is generally dictated by the frequency being used rather than the power of the antenna. Lower frequencies have longer wavelengths, therefore to achieve the same radiation pattern with the same energy, the antenna length must be longer in low frequency communications than high frequency communications. For example, a quarter wave 0 dB gain antenna that is used for the cellular band should be approximately 9 cm. Although the most efficient use of an antenna is subject to one specific frequency, cellular communications use a wide frequency spectrum (824 MHz to 896 MHz for the Cellular band and 1850 to 1960 MHz for the Personal Communications Services - PCS) and sacrifices must therefore be made to make the antenna perform adequately in both bands. This makes dual band antennas less efficient than single band antennas. However, dual band cellular antennas are reasonably efficient and given the reality that cellular phones operate in either band without the users control, it is usually re-

quired that the antenna be as good a radiator as possible in both bands.

Antenna efficiency is significantly improve by the introduction of Ground-plates which provide a reflective effect on all radio frequency signals When an antenna radiates energy, the energy is radiated in all directions. Since radio frequencies do not penetrate highly conductive materials the addition of a reflector enhances the radiative efficiency. Integrated antennas are therefore designed with a built-in ground-plane reflector whereas antennas with coils and symmetrical horizontal protrusions, for example, are designed for use in places where a ground-plane is unavailable. antennas with a built in ground-plane are very effective if they are well designed. Such designs are predicated on the configuration of the antenna and its near-field environment which generates complex interactions due to local scattering effects and it is for this reason that near-field simulation methods are required.

3 Electromagnetic Model

We consider a three-dimensional electromagnetic model based on a medium that is inhomogeneous, isotropic and linear. Isotropy implies that there is no directional bias to the inhomogeneous characteristics of the medium which are scalar functions of space only. Linearity implies that the medium is not affected by the propagation of electromagnetic waves, e.g. it is not a function of the electric or magnetic field strength, for example [13]. Using International Systems of Units (SI) Maxwell's (macroscopic) equations become (e.g. [14] and [15])

$$\nabla \cdot \epsilon \mathbf{E} = \rho, \tag{1}$$

$$\nabla \cdot \mu \mathbf{H} = 0, \tag{2}$$

$$\nabla \times \mathbf{E} = -\mu \frac{\partial \mathbf{H}}{\partial t}, \tag{3}$$

and

$$\nabla \times \mathbf{H} = \epsilon \frac{\partial \mathbf{E}}{\partial t} + \mathbf{j}. \tag{4}$$

where $\mathbf{r} = \hat{\mathbf{x}}x + \hat{\mathbf{y}}y + \hat{\mathbf{z}}z$ is the three-dimensional space vector and t is time, $\mathbf{E}(\mathbf{r}, t)$ is the electric field (volts/metre), $\mathbf{H}(\mathbf{r}, t)$ is the magnetic field (amperes/metre), $\mathbf{j}(\mathbf{r}, t)$ is the current density (amperes/metre^2), $\rho(\mathbf{r}, t)$ is the charge density (charge/metre^2), $\epsilon(\mathbf{r})$ is the permittivity(farads/metre) and $\mu(\mathbf{r})$ is the permeability (henries/metre). The values of ϵ and μ in a vacuum (denoted by ϵ_0 and μ_0, respectively) are $\epsilon_0 = 8.854 \times 10^{-12}$ farads/metre and $\mu_0 = 4\pi \times 10^{-7}$ henries/metre, the relative permittivity ϵ_r and the relative permeability μ_r being defined by $\epsilon_r = \epsilon/\epsilon_0$ and $\mu_r = \mu/\mu_0$, respectively.

Equation (1) is Coulomb's law in differential form. Equation (2) is the law (in differential form) stating that magnetic fields are generated by dipoles (no magnetic monopoles). Equations (3) and (4) are Faraday's and Ampere's laws in differential form, respectively, where, the latter equation includes Maxwell's displacement current term $\epsilon \partial_t \mathbf{E}$. If the medium is considered to be a good conductor and/or consists of isolated conductive elements (such as in an antenna) a current is induced which depends on the magnitude of the electric field and the conductivity σ (siemens/metre) of the material. This allows a further simplification to equation (1) to be made as discussed below.

3.1 Non-Conductive and High Conduction Media

For a linear and isotropic medium, the relationship between the electric field $\mathbf{E}$ and the current density $\mathbf{j}$ is given by Ohm's law

$$\mathbf{j} = \sigma \mathbf{E} \tag{5}$$

Taking the divergence of equation (4) and noting that

$$\nabla \cdot (\nabla \times \mathbf{H}) = 0$$

we obtain (using equation (1) for constant ϵ)

$$\frac{\partial \rho}{\partial t} + \frac{\sigma}{\epsilon} \rho = 0$$

whose solution is

$$\rho(t) = \rho_0 \exp(-\sigma t/\epsilon), \quad \text{where} \quad \rho_0 = \rho(t = 0)$$

which shows that the charge density decays exponentially with time. Typical values of ϵ are $\sim 10^{-12} - 10^{-10}$ farads/metre and hence, if $\sigma >> 1$, the dissipation of charge is very rapid. It is therefore reasonable to set the charge density to zero in equation (1) and, for problems involving the interaction of electromagnetic waves with good conductors, equation (1) becomes

$$\nabla \cdot \epsilon \mathbf{E} = 0 \tag{6}$$

so that equation (4) becomes

$$\nabla \times \mathbf{H} = \epsilon \frac{\partial \mathbf{E}}{\partial t} + \sigma \mathbf{E} \tag{7}$$

On the other hand, if the medium is non-conductive no current can flow so that $\mathbf{j} = 0$ and equation (4) reduces to

$$\nabla \times \mathbf{H} = \epsilon \frac{\partial \mathbf{E}}{\partial t}.$$

On the basis of equations (2), (3), (6) and (7), in Appendix A it is shown that the following inhomogeneous equation for the electric field can by derived:

$$(\nabla^2 + k^2)\widetilde{\mathbf{E}} = -k^2 \gamma_\epsilon \widetilde{\mathbf{E}} + ikz_0 \sigma \widetilde{\mathbf{E}}$$

$$-\nabla(\widetilde{\mathbf{E}}\cdot\nabla\ln\epsilon)-\nabla\times(\gamma_\mu\nabla\times\widetilde{\mathbf{E}}) \quad (8)$$

where

$$\widetilde{\mathbf{E}}(\mathbf{r},\omega)=\int_{-\infty}^{\infty}\mathbf{E}(\mathbf{r},t)\exp(-i\omega t)dt$$

$$k=\frac{2\pi}{\lambda}=\frac{\omega}{c_0},\quad c_0=\frac{1}{\sqrt{\epsilon_0\mu_0}},\quad z_0=\mu_0 c_0,$$

λ is the wavelength and ω is the (angular) frequency of the electric wavefield $\widetilde{\mathbf{E}}$. The parameter z_0 is the free space wave impedance and is approximately equal to 376.6 Ohms and the constant c_0 is the velocity at which electromagnetic waves propagate in a 'free space'. Equation (8) is the basis for developing the three-dimensional simulator reported in this paper.

3.2 Wave Equation for a Constant Dielectric Medium

In principal, a solution to equation (8) can be used to generate the electric wavefield strength given any geometrical antenna design with known functions $\epsilon(\mathbf{r})$, $\mu(\mathbf{r})$ and $\sigma(r)$. However, in most cases, the influence of variations in the permeability can be taken to be insignificant compared to the permittivity and, in particular, the conductivity, when concerned with the design of an antenna. For a 'conductivity only' model, where the permittivity and permeability are taken to be constant, equation (8) reduces to the form

$$(\nabla^2+k^2)\widetilde{\mathbf{E}}=ikz_0\sigma\widetilde{\mathbf{E}}$$

Apart from removing three terms from the the right hand side of equation (8), this model also allows a solution to be developed using a scalar wave equation since the equation above applies to any vector component of the electric field. However, this is also the case if we ignore polarisation effects induced by variations in the permittivity due to the term $\nabla(\widetilde{\mathbf{E}}\cdot\nabla\ln\epsilon)$ and use the equation

$$(\nabla^2+k^2)\widetilde{\mathbf{E}}=-k^2\gamma_\epsilon\widetilde{\mathbf{E}}+ikz_0\sigma\widetilde{\mathbf{E}}$$

Thus, we consider a solution to the scalar wave equation

$$(\nabla^2+k^2)u(\mathbf{r},k)=-\Gamma(\mathbf{r},k)u(\mathbf{r},k)-s(\mathbf{r},k)$$

for constant k where u is any component of the electric wavefield vector,

$$\Gamma(\mathbf{r},k)=k^2\gamma_\epsilon(\mathbf{r})-ikz_0\sigma(\mathbf{r})$$

and s is a source function which is taken to describe the 'primary source' of electromagnetic radiation in the antenna. The inclusion of the source term provides a source-scattering model in which the wavefield u is taken to be the sum of the incident field u_i generated by the primary source and the scattered field u_s generated by the interaction of this incident field within the (near-field) vicinity of the antenna. This effect is important when designing integrated antennas as discussed in Section I and is the ficus of the work reported herein.

The incident field is given by the solution of

$$(\nabla^2+k^2)u_i(\mathbf{r},k)=-s(\mathbf{r},k) \quad (9)$$

so that the scattered field can be taken to be given by the solution of

$$(\nabla^2+k^2)u_s(\mathbf{r},k)=-\Gamma(\mathbf{r},k)u(\mathbf{r},k) \quad (10)$$

where

$$u(\mathbf{r},k)=u_i(\mathbf{r},k)+u_s(\mathbf{r},k)$$

In each case, we consider the dielectric parameters to be real and of compact support in real space, i.e. $\mathbf{r}\in\mathbb{R}^3$.

4 Green's Function Solutions

The general solutions to equations (9) and (10) using the free space Green's function method are well known and given by [17]

$$u_i(\mathbf{r},k)=\oint_{\mathcal{S}}(g\nabla u_i-u_i\nabla g)\cdot d^2\mathbf{r}+g(\mathbf{r},k)\otimes_3 s(\mathbf{r},k) \quad (11)$$

and

$$u_s(\mathbf{r},k)=\oint_{\mathcal{S}}(g\nabla u_s-u_s\nabla g)\cdot d^2\mathbf{r}+g(\mathbf{r},k)\otimes_3\Gamma(\mathbf{r})u(\mathbf{r},k) \quad (12)$$

respectively, where g is the Green's

$$g(r,k)=\frac{\exp(ikr)}{4\pi r}$$

which is the solution to

$$(\nabla^2+k^2)g(r,k)=-\delta^3(r)$$

and $\otimes_3$ denotes the three-dimensional convolution integral

$$g(\mathbf{r})\otimes_3 f(\mathbf{r})=\int_{\mathbb{R}^3}g(\mid\mathbf{r}-\mathbf{r}'\mid)f(\mathbf{r}')d^3\mathbf{r}'$$

The surface integrals (obtained through application of Green's Theorem) represent the effect generated by a boundary upon which the fields u_i and u_s. These fields together with their respective gradients need to be specified - the 'Boundary Conditions'. In the case of equation (11), the surface integral determines the effect of the surface of the source when it is taken to be of compact support. With regard to equation (12), the surface integral

models surface scattering effects. In the context of the model considered here, the surface integrals are taken to be zero so that volume effects are considered alone. Formally, this requires that we invoke the 'homogeneous boundary condition'

$$u_i = 0, \quad u_s = 0, \quad \nabla u_i = \mathbf{0} \quad and \quad \nabla u_s = \mathbf{0}$$

and equation (12) is reduced to

$$u_s(\mathbf{r}, k) = g(\mathbf{r}, k) \otimes_3 \Gamma(\mathbf{r}.k) u(\mathbf{r}, k) \tag{13}$$

which is the solution to equation (10) since

$$(\nabla^2 + k^2) u_s(\mathbf{r}, k) = (\nabla^2 + k^2)[g(\mathbf{r}, k) \otimes_3 \Gamma u(\mathbf{r}, k)]$$
$$= -\delta^3(\mathbf{r}) \otimes_3 \Gamma(\mathbf{r}.k) u(\mathbf{r}, k) = -\Gamma(\mathbf{r}, k) u(\mathbf{r}, k)$$

We require a solution for u_s given equation (13) which has the conventional iterative form (for $n = 0, 1, 2, ...$)

$$u_s^{(n+1)}(\mathbf{r}, k) = g(\mathbf{r}, k) \otimes_3 \Gamma u_i(\mathbf{r}, k) + g(\mathbf{r}, k) \otimes_3 \Gamma u_s^{(n)}(\mathbf{r}, k)$$

where $u_s^{(0)}(\mathbf{r}, k) = 0$ leading to the Born series given by

$$u_s = g \otimes_3 \Gamma u_i + g \otimes_3 [\Gamma(g \otimes_3 \Gamma u_i)] + ... \tag{14}$$

each term representing the effect of single, double and high order scattering effect respectively [18]. The first term $g \otimes_3 \Gamma u_i$ provides a solution under the Born approximation when $\|u_s\| << \|u_i\|$ and implies that

$$\langle \Gamma \rangle \equiv \sqrt{\frac{\int\limits_{\mathbb{R}^3} |\ \Gamma\ |^2\, d^3\mathbf{r}}{\int\limits_{\mathbb{R}^3} d^3\mathbf{r}}} << \frac{1}{R^2}$$

where R is the radius of a sphere whose volume is taken to be equal to that of the scattering domain $\mathbb{R}^3$.

For 800 - 2400 MHz transmission frequencies used by cell phones, the wavelength is approximately 0.3 metres and if we take $R \sim 0.03$ metres (i.e. a scattering domain on the cm scale) then, using the definition of Γ, this condition becomes

$$\langle \gamma_\epsilon - 18 i\sigma \rangle << 2.5$$

which is not easily satisfied for arbitrary geometries of the permittivity and conductivity especially if these values are high (the conductivity of metals being $\sim 10^7$ siemens per metre). On the other hand, if we consider a scattering domain to be composed of 'infinitely thin' components such as a patch antenna and reflector (as considered in Section VI and Section VII) then the scattering domain is taken to be composed primarily empty space and the condition above is more easily satisfied. However, there is another approach that can be taken to evaluate the scattered field u_s. This is based on noting that, because [19], [20]

$$\nabla^2 \frac{1}{4\pi r} = -\delta^3(r)$$

then

$$(\nabla^2 + k^2) u_s(\mathbf{r}, k) = \nabla^2 \left(u_s - \frac{k^2}{4\pi r} \otimes_3 u_s \right)$$

and equation (10) can be written in the form of the inhomogeneous Poisson equation

$$\nabla^2 \left[u_s(\mathbf{r}, k) - \frac{k^2}{4\pi r} \otimes_3 u_s(\mathbf{r}, k) \right]$$
$$= -\Gamma(\mathbf{r}, k) u_i(\mathbf{r}, k) - \Gamma(\mathbf{r}, k) u_s(\mathbf{r}, k)$$

which has the Green's function solution

$$\left[u_s(\mathbf{r}, k) - \frac{k^2}{4\pi r} \otimes_3 u_s(\mathbf{r}, k) \right]$$
$$= \frac{1}{4\pi r} \otimes_3 \Gamma(\mathbf{r}, k) u_i(\mathbf{r}, k) + \frac{1}{4\pi r} \otimes_3 \Gamma(\mathbf{r}, k) u_s(\mathbf{r}, k)$$

subject to the homogeneous boundary conditions for the Green's function $(4\pi r)^{-1}$. Collecting like terms, we can now write

$$u_s(\mathbf{r}, k) = \frac{1}{4\pi r} \otimes_3 \Gamma(\mathbf{r}, k) u_i(\mathbf{r}, k)$$
$$+ \frac{1}{4\pi r} \otimes_3 [k^2 + \Gamma(\mathbf{r}, k)] u_s(\mathbf{r}, k) \tag{15}$$

Both equation (13) and equation (15) are solutions to equation (10) since, in the latter case, taking the Laplacian of equation (14),

$$\nabla^2 u_s(\mathbf{r}, k) = \nabla^2 \frac{1}{4\pi r} \otimes_3 \Gamma(\mathbf{r}, k) u_i(\mathbf{r}, k)$$
$$+ \nabla^2 \frac{1}{4\pi r} \otimes_3 [k^2 + \Gamma(\mathbf{r}, k)] u_s(\mathbf{r}, k)$$
$$= -\delta^3(\mathbf{r}) \otimes_3 \Gamma(\mathbf{r}, k) u_i(\mathbf{r}, k) - \delta^3(\mathbf{r}) \otimes_3 [k^2 + \Gamma(\mathbf{r}, k)] u_s(\mathbf{r}, k)$$
$$= -\Gamma(\mathbf{r}, k) u_i(\mathbf{r}, k) - k^2 u_s(\mathbf{r}, k) - \Gamma(\mathbf{r}, k) u_s(\mathbf{r}, k)$$

However, in the case of equation (15), we can consider the iteration

$$u_s^{(n+1)}(\mathbf{r}, k) = \frac{1}{4\pi r} \otimes_3 \Gamma(\mathbf{r}, k) u_i(\mathbf{r}, k)$$
$$+ \frac{1}{4\pi r} \otimes_3 [k^2 + \Gamma(\mathbf{r}, k)] u_s^{(n)}(\mathbf{r}, k)$$

which yields the series solution

$$u_s = \frac{1}{4\pi r} \otimes_3 \Gamma u_i + \frac{1}{4\pi r} \otimes_3 \left[(k^2 + \Gamma) \frac{1}{4\pi r} \otimes_3 \Gamma u_i \right] + ... \tag{16}$$

Taking the first term in equation (16) is then the equivalent of applying the Born approximation to compute the scattered field given equation (14). However, this solution shows that all higher order terms in equation (16), which represent multiple scattering effects by analogy with equation (14), vanish if (the 'null multiple scattering condition')

$$k^2 + \Gamma(\mathbf{r}, k) = 0, \quad \forall \mathbf{r} \in \mathbb{R}^3$$

This is an entirely different condition to that required to apply the Born approximation to equation (14) - the conventional solution method - although predicated on a scalar wavefield theory in which polarisation effects are ignored. Nevertheless, under this condition, the Born approximation becomes an exact solution and, by inference, inverse solutions (under the Born approximation) become exact solutions[1] The condition above states that

$$k\epsilon_r(\mathbf{r}) - iz_0\sigma(\mathbf{r})$$

$$= \sqrt{k^2\epsilon_r^2(\mathbf{r}) + z_0^2\sigma^2(\mathbf{r})}\exp[-i\theta(\mathbf{r}, k)] = 0, \quad \forall \mathbf{r} \in \mathbb{R}^3$$

where

$$\theta(\mathbf{r}, k) = \tan^{-1}\left[\frac{z_0\sigma(\mathbf{r})}{k\epsilon_r(\mathbf{r})}\right]$$

and is therefore satisfied if (for any integer n)

$$\theta(\mathbf{r}, k) = \pm\frac{n\pi}{2} \quad \text{and} \quad \pm n\pi,$$

a duality which is not plausible, or

$$k^2\epsilon_r^2(\mathbf{r}) + z_0^2\sigma^2(\mathbf{r}) = 0$$

$$\Rightarrow \quad \sigma(\mathbf{r}) = \pm\frac{ik\epsilon_r(\mathbf{r})}{z_0} = \pm i0.0167\frac{\epsilon_r(\mathbf{r})}{\lambda}$$

In the latter case, there exists the implication that the relative permittivity can be both positive and negative. The negative option being associated with 'negative index' materials, e.g. [21]. More specifically, the condition (which requires that the conductivity is imaginary) reduces equation (15) to

$$u_s(\mathbf{r}, k) = \frac{1}{4\pi r} \otimes_3 f(\mathbf{r})u_i(\mathbf{r}, k)$$

where

$$f(\mathbf{r}) = \begin{cases} 1. & \forall \mathbf{r} \in \mathbb{R}^3; \\ 0, & \forall \mathbf{r} \notin \mathbb{R}^3. \end{cases}$$

Note, that this 'null multiple scattering condition' does not affect the geometry and topology of the binary 'scattering function' $f(\mathbf{r})$ which can be completely arbitrary in terms of its simplicity .v. complexity.

[1]The condition $k = 0$ represents the trivial case consistent with the condition' $k \to 0$ when the conventional Born approximation becomes an exact solution to the problem - the 'Ramm Scattering' condition.

5 Solutions for the Scattered field in the Fresnel and Fourier Zones

Evaluating the scattered field in the Fresnel and Fourier zones is well known in the case of equation (14). However, equation (16) provides properties that simplify this evaluation as shown below. We consider the case when the source function is a delta function so that incident field u_i is given by the Green's function

$$g(\mid \mathbf{r} - \mathbf{r}_0 \mid, k) = \frac{\exp(ik \mid \mathbf{r} - \mathbf{r}_0 \mid)}{4\pi \mid \mathbf{r} - \mathbf{r}_0 \mid}$$

where $\mathbf{r}$ is taken to be the position of the source and $\mathbf{r}_0$ is the point at which the wavefield is observed It is well known that the key to evaluating the scattered field in the Fresnel and Fourier zones relies on a binomial expansion of $\mid \mathbf{r} - \mathbf{r}_0 \mid$ in the exponential component of the Green's function and considering the relative magnitudes of the vectors $\mathbf{r}$ and $\mathbf{r}_0$ (given by r and r_0, respectively). This yields the results given in the following sections.

5.1 Fourier Zone

$$g(\mathbf{r}, \mathbf{r}_0, k) = \frac{1}{4\pi r_0}\exp(ikr_0)\exp(-ik\hat{\mathbf{n}} \cdot \mathbf{r}), \quad \hat{\mathbf{n}} = \frac{\mathbf{r}_0}{\mid \mathbf{r}_0 \mid}$$

which is based on the condition $r/r_0 << 1$ so that terms involving second and high order powers of this quotient are ignored. In equation (16), the convolution terms become integrals over $\mathbf{r} \in \mathbb{R}^3$ (where r_0 is taken to be outside of the domain of integration) and we obtain the result

$$u_s(\mathbf{r}_0, k) = c(r_0, k)\frac{\exp(ikr_0)}{(4\pi r_0)^2}A(\hat{\mathbf{n}}, k)$$

where A is the scattering amplitude given by

$$A(\hat{\mathbf{n}}, k) = \int_{\mathbb{R}^3} \Gamma(\mathbf{r}, k)\exp(-ik\hat{\mathbf{n}} \cdot \mathbf{r})d^3\mathbf{r} \tag{17}$$

and

$$c(r_0, k) = \left(1 + \frac{1}{4\pi r_0}\int_{\mathbb{R}^3}[k^2 + \Gamma(\mathbf{r}, k)]d^3\mathbf{r} + ...\right) \tag{18}$$

5.2 Fresnel Zone

$$g(\mathbf{r}, \mathbf{r}_0, k) = \frac{1}{4\pi r_0}\exp(ikr_0)\exp(-ik\hat{\mathbf{n}} \cdot \mathbf{r})\exp(i\alpha r^2)$$

where

$$\alpha = \frac{k}{2r_0} = \frac{\pi}{\lambda r_0}$$

which is based on relaxing the condition $r/r_0 << 1$ and ignoring all terms with higher order powers greater than 2. In this case, equation (16) becomes

$$u_s(\mathbf{r}_0,k) = c(r_0,k)\frac{\exp(ikr_0)}{(4\pi r_0)^2}$$

$$\times \int_{\mathbb{R}^3} \Gamma(\mathbf{r},k)\exp(-ik\hat{\mathbf{n}}\cdot\mathbf{r})\exp(i\alpha r^2)d^3\mathbf{r}$$

However, noting that

$$\frac{ik}{2r_0} \mid \mathbf{r}_0 - \mathbf{r} \mid^2 = \frac{ik}{2r_0}(r_0^2 + r^2 - 2\mathbf{r}_0\cdot\mathbf{r})$$

$$= \frac{ikr_0}{2} + \frac{ikr^2}{2r_0} - ik\hat{\mathbf{n}}\cdot\mathbf{r}$$

we can write this result in the form

$$u_s(\mathbf{r},\mathbf{r}_0,k) = c(r_0,k)\frac{\exp(ikr_0/2)}{(4\pi r_0)^2}A(\mathbf{r},k)$$

where A is the scattering amplitude function given by

$$A(\mathbf{r},k) = \Gamma(\mathbf{r},k) \otimes_3 \exp(i\alpha r^2) \tag{19}$$

the function $\exp(i\alpha r^2)$ being the (three-dimensional) Fresnel Point Spread Function (PSF).

Equations (17) and (19) represent the scattering amplitude generated in the 'far' and 'intermediate' fields, respectively. The complex coefficient $c(r_0,k)$ incorporates the multiple scattering effects that are determined by the integral of the function $k^2 + \Gamma(\mathbf{r},k)$ over the scattering domain $\mathbb{R}^3$. However, the value of this coefficient does not affect the models for the scattering amplitudes given by equations (17) and (19) and it is clear that the series defining this coefficient will converge provide

$$\frac{1}{4\pi r_0}\left| \int_{\mathbb{R}^3} [k^2 + \Gamma(\mathbf{r},k)]d^3\mathbf{r} \right| < 1$$

6 Radiation Field Patterns for a Simple Monopole Source

The design of an integrated antenna for a given application ultimately depends on the interaction of electromagnetic waves generated by a primary source whose physical size with respect to the wavelength has the predominant influence on the radiation characteristics. With modern day communication devices becoming smaller and lighter, demand for low-profile antenna designs has increased. One way of realising a low-profile antenna design is to use a high impedance ground plane in place of the conventional metallic ground plane. Metallic plates are used as ground planes to redirect the back-scattered radiation and provide shielding to the antennas. Conventional ground planes that are Perfect Electric Conductors (PECs) exhibit the property of phase reversal of the incident currents that result in destructive interference of both the original antenna currents and the image currents. To overcome this effect, antennas are placed at a quarter wavelength above the metallic ground plane, making the size of the antenna bulky at low frequencies. To reduce the size of the antenna, a ground plane that is a dual of the conventional PECs is needed, i.e. a perfect magnetic conductor is required. This is achieved by introducing a High Impedance Surface (HIS) which can be considered to be an artificial magnetic conductor. HISs are popular for their widespread applications in reflected array antennas, low-profile antennas, electromagnetic absorbers and polarisers. These surfaces exhibit unique properties such as the in-phase reflection of incident waves and the suppression of surface waves. Different antenna parameters such as gain, impedance and size can be enhanced by incorporating the HISs into the antenna structures. Thus, the back-scattering of radiation from a high impedance back-reflector is an important factor in the simulation of the resulting radiation field pattern and must be undertaken in the near field.

We consider the interaction of the electric wavefield in the Fresnel zone for an antenna composed of an array-reflector system based on evaluating equation (19) for the positive half space, the reflector being placed at the origin of the half-space $z > 0$. The far-field radiation pattern is then given by the Fourier transform of the resulting wavefield which is taken to be the source of radiation generated by the scattering of the electric wavefield between the primary antenna and the back-reflector (in the Fresnel zone), the intensity field pattern being given by

$$I(\hat{\mathbf{n}}.k) = \mid \widetilde{A}(\hat{\mathbf{n}},k) \mid^2 \tag{20}$$

where

$$\widetilde{A}(\hat{\mathbf{n}},k) = \int_{\mathbb{R}^3} A(\mathbf{r},k)\exp(-ik\hat{\mathbf{n}}\cdot\mathbf{r})d^3\mathbf{r}$$

and $A(\mathbf{r},k)$ is defined by equation (19).

We consider a digital computation using a regular three-dimensional Cartesian mesh of size N^3 where the antenna is placed at a fixed distance $z = L$ voxels from the primary reflector and taken to have a thickness of 1 Voxel[2]. Further, for simplicity with regard to developing a first illustrative example, we consider an integrated antenna to be composed of conductive elements alone with uniform

[2]A 'Voxel' is a Volume Element.

conductivity where the permittivity of the scattering domain $\mathbb{R}^3$ is 1 so that $\Gamma(x, y, z) = ikz_0\sigma(x, y, z)$. For a fixed wavelength, the complex coefficient ikz_0 is not relevant to the computation of the intensity field pattern given by equation (20) which is normalised for display purposes. In this context, the value of σ can be taken to be equal to 1 for all Voxels that describe the geometry of the the antenna including the primary back-reflector within the scattering domain $\mathbb{R}^3$.

Computation of the Fresnel PSF is also undertaken on a Cartesian grid. For a given value of N, the scaling of this function (i.e. the range of values of α that can be applied) is important in order to avoid aliasing. For the current application, the scaling can be based on considering the resonance frequency condition discussed in Section I. Under this condition, we require the size of the antenna to be approximately one quarter of a wavelength. For a patch antenna, which is taken to infinitely thin in the scattering domain, we then require that

$$\frac{\lambda}{4} \sim \Delta N$$

where Δ defines the spatial resolution of the mesh, the length of each side of a Voxel being taken to be given by Δ. Thus,

$$\alpha r^2 = \frac{\pi}{\lambda r_0}\Delta^2(n_x^2 + n_y^2 + n_z^2)$$

where n_x, n_y, and n_z are array indices running from $-N/2$ through 0 to $N/2$, the Fresnel PSF being computed over all space and not just a positive half-space. It is then clear that we can obtain a wavelength independent (a consequence of the resonance condition) expression for α given by

$$\alpha = \frac{4\pi}{N}\frac{\Delta}{r_0}$$

Figure 2 shows a simple example for an idealised monopole antenna composed of a single circular element (with no feed contacts) and a reflector which are both taken to be 'infinitely thin' placed $L = 10$ Voxels apart. The element is taken to radiate a electric wavefield which back-scatters from the back-reflector to produce a field pattern determined by equation (19). This field pattern is based on scattering effects generated by both the back-reflector and the primary radiation source. The scattered wavefield generated within $\mathbb{R}^3$ establishes a secondary radiation source whose far-field intensity field pattern is then given by equation (20). This produces a different field pattern to that modelled by treating the antenna as a source function alone and computing the Fourier transform of this function to evaluate the radiation field intensity in the far-field.

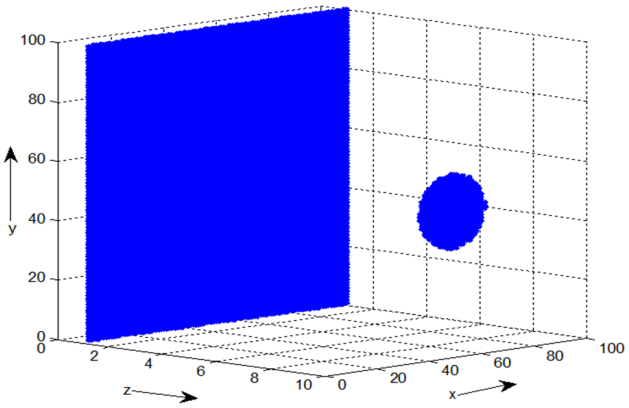

Figure 2: Basic three-dimensional geometry of an idealised antenna consisting of a single circular element (the source function in absence of feed contacts) with a thickness of 1 Voxel placed 10 Voxels from a back-reflector also with a thickness of 1 Voxel using a 100^3 Cartesian mesh.

Figure 3 shows an Iso-surface of the Fresnel PDF for $\Delta/r_0 = 0.1$ and illustrates the three-dimensional wave fronts generated by a function with a quadratic phase that is a 'near-field characteristic'.

Figure 4 shows a colour coded normalised intensity map of the field $\mid A(x, y, z = 2L) \mid^2$ obtained by convolving the PDF given in Figure 3 with the scattering function given in Figure 2 using the MATLAB function *convn* with the option 'same' which returns the central part of the convolution that is the same size as the input arrays.

If we now take the field in the plane at $z = 2L$ to be a (planar source) then the far-field intensity pattern is given by taking the two-dimensional Fourier transform of the function $A(x, y, z = 2L)$. This is shown in Figure 5 which provides normalised colour coded maps of the log power spectrum and, for comparison, the log power spectrum of the source function alone (i.e. the antenna element without the back-reflector), the axes being given by $(kx_0/z_0, ky_0/z_0)$[3]. As expected, there is a significant difference between these field patterns especially with regard to their comparative intensities away from the central lobe due to the Fresnel interaction of the source with the back-reflector. The spectrum of the source function alone (an infinitely thin circular disc) shows an 'Airy pattern' characterised by the function $J_1(ka)/(ka)$ where a is the radius of the disc and J_1 is the first order Bessel

[3]Computed using the MATLAB function *fft2* with *fftshift* which generates a two-dimensional Fourier transform in 'optical form' with the zero-frequency component placed at the centre of the spectrum.

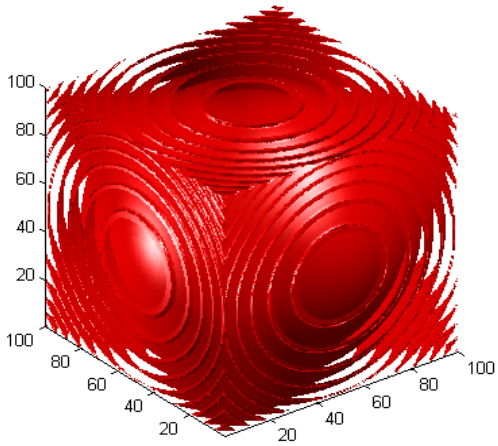

Figure 3: Isosurface of the Fresnel PSF given in equation (19) using a 100^3 Cartesian mesh with $\Delta/r_0 = 0.1$.

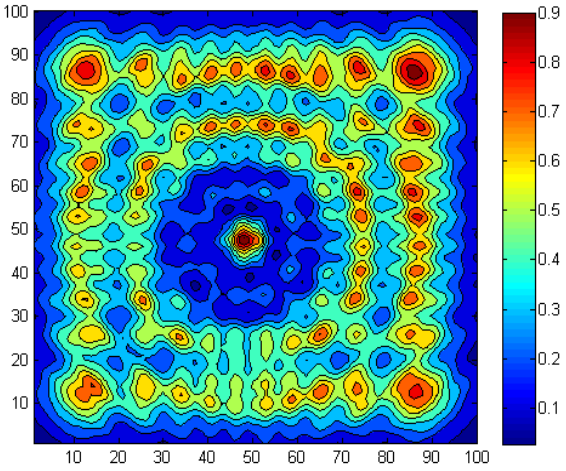

Figure 4: Intensity field map of the function given by equation (19) for $z = 5L$.

function of the first kind. This function describes a circularly symmetric spectrum composed of a central lobe surrounded by a sequence of concentric rings separated by the positions at which the Bessel function approaches zero.

The three-dimensional field patterns can of course be investigated by computing the three-dimensional Fourier transform as given by equation (20) and visualised at different planes and/or different coordinate geometries. The results given in Figure 5 are illustrative of the near-field scattering effects generated by the interaction of a primitive source-reflector system. In the context of the model considered, given a specific antenna and back-reflector geometry (with uniform conductivity), the field patterns are determined by the parameter set $(L, \Delta/r_0)$. This parameter set does not affect simulations in the far-field obtained by taking the Fourier transform of the source function alone.

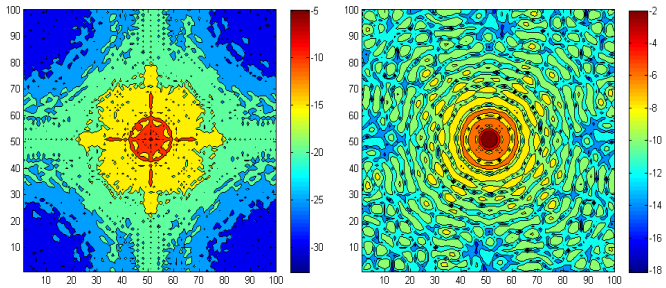

Figure 5: Log Power Spectrum of the field whose intensity map is given in Figure 4 (left) and the Log Power Spectrum of the source function shown in Figure 2 (right).

7 Fields Generated by Fractal Antennas

The method of simulation discussed in the previous section can be used to simulate the field patterns generated by any integrated antenna configuration coupled with near field components. A Voxel modelling system is required to construct three-dimensional arrays representing the conductivity and the permittivity of the integrated source-reflector (or otherwise) antenna system details of which lie beyond the scope of this paper. However, it should be noted that, unlike the example given in the previous section, a Volume element model for Γ which includes variations in both the permittivity and conductivity (which yields a complex scattering function) generates cross-terms in the radiation field pattern since, from equation (19), the scattered amplitude intensity is given by

$$\mid A(\mathbf{r}, k) \mid^2 = k^4 \mid [\gamma_\epsilon(\mathbf{r}) - i(z_0/k)\sigma(\mathbf{r})] \otimes_3 \exp(i\alpha r^2) \mid^2$$

The geometries of planar antennas are becoming increasingly complex and include fractal geometric shapes which exhibit self-similar or fractal properties which are compact designs [22]. These antennas have radiative elements that contain at least one multi-level structure formed by a set of similar geometric elements (polygons or polyhedrons) electromagnetically coupled and grouped such that the structure of the antenna can be identified by each of the basic component elements. The design provides two important advantages: the antenna may operate simultaneously in several frequencies, and/or its size can be substantially reduced. Thus, a multi-band radio-electric behaviour is achieved, providing similar behaviour for different frequency bands. Planar arrays of periodic resonant elements (printed or complementary slot) interact with electromagnetic waves within certain frequency band(s) and can be characterised as Frequency Selective Surfaces (FSS). Different FSS elements have been described in the literature, where each design has its own advantage over the other. The overall goal of fractal antennas design is the realisation of the 'Rumsey Principle' which is that the impedance and pattern properties of an antenna will be frequency independent if the shape is specified only in terms of angles.

Fractal antenna have been developed commercially since the 2000 [23] and include a range of strictly fractal and quasi-fractal types some of which are based on well known fractal shapes such as the Sierpinski gasket [24] and von Koch monopole [25]. Some conventional wide-band antennas can be considered to fall into the class of fractal structures. For example, the logarithmic spiral and log-periodic structures can be considered as fractal antennas The infinite (logarithmic) spiral is a constant impedance device over all frequencies and we can consider the spiral as 'smoothly' self-symmetric. The Log-Periodic Dipole Array (LPDA) is a wide-band device (actually it is multi-band with arbitrarily close band spacing). Its various performance properties repeat in the same geometric ratio (log-periodic) with regard to element size and spacing. The LPDA is an example of a 'discretely' self-symmetric antenna.

The principal reason for the multi-modal and broad-band characteristics of fractal antennas is the space filling properties of fractals. For this reason antennas designed from certain fractal shapes can have superior electrical to physical size ratios than antennas designed from an understanding of shapes based on Euclidean geometry including those designed from free form curves/surfaces. This effect is not exclusive to deterministic fractals and random scaling fractal arrays can be used to balance long-range order (typical of fractals) and short-range disorder (typical of random arrays). The randomness provides robustness to element failure while the fractal structure provides the required multi-band or wide-band performance. Moreover, unlike deterministic fractals (which have a specific fractal dimension) random fractal arrays [26] can be used to produce fractal radiation patterns for user defined values of the Fractal Dimension D.

By way of an example, Figure 6 shows simulations of the field intensities generated in the plane for the Sierpinski Carpet antenna (which has a Fractal Dimension $D = 1.8928$) and is illustrative of the different modes generated by the electric field scattering from a plane reflector at different distance from the antenna.

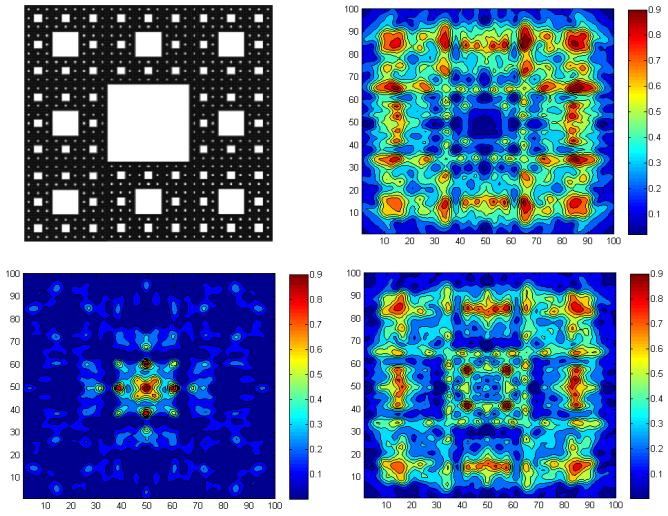

Figure 6: Fractal antenna (top-left) and the Fresnel zone radiation patterns in the plane at $z = 2L$ using a 100^3 mesh for $L = 5, 10$ and 15 with $\Delta/r_0 = 0.1$.

Another property that is easily investigated is the (scalar) current density j induced though the scattered electric field E in the plane of the antenna since from Ohms law $j(x, y) = \sigma(x, y)E(x, y) \sim \sigma(x, y)A(x, y)$. In practice, the current density is obtained by multiplying the antenna array with the field pattern generated in the plane at which the antenna is placed. By way of an example, Figure 7 shows the induction currents generated for the Sierpinski Carpet and Quadratic Snow Flake ($D = 1.37$) antennas.

8 Summary

The purpose of this paper has been to develop a three-dimensional simulator for investigating the scattering electromagnetic field generated by an integrated antenna. The model has been derived in a systematic fashion start-

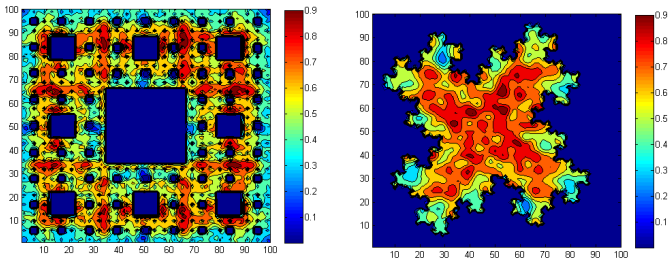

Figure 7: Induction currents induced by the scattered electric field in the Sierpinski Carpet (left) and Quadratic Snow Flake (right) antennas for $L = 10$ and $\Delta/r_0 = 0.1$.

ing with Maxwell's macroscopic equation so that the conditions upon which the present simulator is based are clearly identified in terms of fundamental electromagnetic theory. The focus of the model has been to introduce the volume scattering effects generated by the integration of an antenna into a compact space associated with the design of a mobile phones, for example. In this case, the antenna can not be assumed to be an isolated radiative source and simulation of the radiation field pattern based on the use of a source function alone is not valid. In this paper, we have considered the locality of an integrated antenna to be a scattering environment in the near field. The scattered field is then taken to be the source of radiation whose far-field radiation pattern is obtained through Fourier transformation. However, like all simulation methods there are limits imposed on the applied physics of the model used. The conditions used in the work report in this paper are as follows:

- the dielectric material is isotropic and assumed to be composed of (three-dimensional) variations in the permittivity and conductivity alone;
- the magnetic permeability is taken to be a constant so that the term $\nabla \times (\gamma_\mu \nabla \times \mathbf{E})$ given in equation (8) can be ignored;
- polarisation effects due to variations in the permittivity which are compounded in the term $\nabla(\mathbf{E}\cdot\nabla \ln \epsilon)$ given in equation (8) are ignored.

However, within the context of the model developed, whose principal conditions are listed below, it is relatively easy to include these terms in order to investigate polarisation effects (through variations in the relative permittivity and/or variations in the relative permeability) which will be the subject of a future publication.

The principal conditions upon which the scattered field is evaluated are as follows:

1. the scattered field is a model for the electric field alone;
2. surface scattering is negligible (homogenous boundary condition are imposed) and the simulator is based strictly on a volume scattering model;
3. multiple scattering effects are insignificant at least within the near-field domain over which the the scattered field is evaluated;
4. scattering occurs in the Fresnel zone where the wavefronts are taken to have a quadratic phase;
5. computation of the scattered field is based on using the quarter wavelength resonance frequency condition so that the Fresnel PSF become wavelength independent.

With regard to surface scattering effects, it is noted that the skin depth (the depth below the surface of a conductor at which the electric field has decade to $1/e \simeq 0.37$ of the field at the surface) is given by $\delta = \sqrt{\lambda/(\pi\mu\sigma)}$. For non-conductive dielectrics, volume scattering dominates but for conductive dielectrics the effect of volume versus surface scattering is determined by the depth to which the electric field penetrates the material. For wavelengths of the order of 0.3 metres and with $\mu\sigma \sim 1$ (N.B. averaged over the scattering domain), the skin depth is approximately 0.3 metres. Thus, the volume scattering condition is appropriate given that the dimensions of an integrated antenna and the volume of the scattering domain are on the same scale. Moreover, for patch antennas whose dimensions are comparable to the skin depth (and taken to be infinitely thin, at least on a theoretical basis), surface scattering effects are not as significant as volume scattering. Moreover, surface scattering requires that the surface integrals and hence, surface patches, have to be defined precisely and the generality afforded by a volume scattering simulation in terms of utilising a Voxel based Computer Aided Design system, is not applicable.

In terms of the conditions 1-5 above, the issue of neglecting multiple scattering effects is a fundamental issue with regard to all electromagnetic and other wave scattering models. In this paper we have considered a solution based on the conventional Green's function solution to the inhomogeneous Helmholtz equation and compared the result with a Green's function solution to the inhomogeneous Poisson equation based on an equivalence relationship for the Helmholtz operator. The latter solution reveals a 'null multiple-scattering condition' that is not apparent

using the former conventional approach and warrants further investigation into its ramifications in terms of, for example, the possibility of designing integrated antenna using conductive meta-materials that generate plasmon resonance and eliminate dissipation through multiple scattering. Application of the Fresnel zone to model near-field scattering provides a model that is based on convolving the scattering function with the Fresnel PSF compounded in the expression for the scattering amplitude given by equation (19). The principle 'computational cost' is then determined by the discrete convolution operation required to evaluate this equation on a high resolution mesh where the PSF is conditioned by applying the quarter wavelength resonance effect which integrated antennas used to boost the signal.

With regard to the computational issues discussed in this paper and the result presented, there is significant potential for the development of a sophisticated Voxel modelling system for designing integrated antennas with variations in the permittivity, permeability and conductivity each subject to a geometry of a arbitrary complexity. However, this is predicated on the computational performance being available to evaluate equation (19) over a three-dimensional mesh having a resolution that is compatible with the geometric detail of the antenna. In this way, the approach considered in this paper can be used to assess the near- and then far-field radiation patterns generated by a given design in order to optimise the performance of mobile communications devices. Finally, the approach can be extended to simulate time dependent problems by taking the incident field to be given by

$$u_i(\mathbf{r}, k) = P(k)g(r, k)$$

where $P(k), \quad k = \omega/c_0$ is the temporal Transfer Function with band-width Ω and Impulse Response Function (IRF)

$$p(t) = \frac{1}{2\pi} \int_{-\Omega/2}^{\Omega/2} P(\omega) \exp(i\omega t) d\omega$$

From equation (19), the time dependent signal associated with the near-field scattering amplitude is then given by

$$s(\mathbf{r}, t) = p(t) \otimes_t \frac{\Omega}{2\pi} \mathrm{sinc}(\Omega t/2) \otimes_t a(\mathbf{r}, t)$$

where

$$a(\mathbf{r}, t) = \frac{1}{2\pi} \int_{-\infty}^{\infty} A(\mathbf{r}, \omega) \exp(i\omega t) d\omega$$

and $\otimes_t$ denotes the convolution integral over time t, the far-field (time-dependent) intensity pattern being obtained through application of equation (20).

Time-dependent analysis is important in the design of Ultra-Wide-Bband (UWB) antennas [6] which are often used for short range, indoor transmission due to low emission requirements and where short pulse lengths enable transmission of high data rate signals [27]. The IRF is typically given by a modulated Gaussian pulse and applications include high precision through-wall radar imaging and PC-peripherals such as wireless printers. In such cases, additional time domain analysis is necessary to characterise the antennas overall performance for pulsed signal transmission. Parameters such as pulse distortion and antenna fidelity need to be analysed together with standard antenna performance parameters for reliable design [28]. Near- and far-field radiation patterns generated by UWBs are consider in [29] using a similar approach to that considered in this paper.

By focusing on a volume scattering approach to compute near-field effects compounded in equation (19), emphasis can be placed on integrated antenna designs using Voxel modelling systems such as *Voxelogic* [30] and *Voxel Sculpting* [31] that allow designers to sculpt without any topological constraints. These systems include open source produce such as *VoxCAD* [32] that provides for the inclusion of multiple materials and is therefore ideal for introducing designs based on variations in the relative permittivity, relative permeability and conductivity. Systems such as *Pendix*, [33] operate like 2D graphics software while producing 3D models, [34] and are therefore ideal for designing single material based patch antennas.

Appendix A: Derivation of the Wave Equation for an Electric Field

By decoupling Maxwell's equations for the magnetic field $\mathbf{H}$, a wave equation for the electric field $\mathbf{E}$ is recovered. Starting with equation (3), we divide through by μ and take the curl of the resulting equation. This gives

$$\nabla \times \left(\frac{1}{\mu} \nabla \times \mathbf{E} \right) = -\frac{\partial}{\partial t} \nabla \times \mathbf{H}$$

By taking the derivative with respect to time t of equation (4) and using Ohm's law - equation (5) - we obtain

$$\frac{\partial}{\partial t}(\nabla \times \mathbf{H}) = \epsilon \frac{\partial^2 \mathbf{E}}{\partial t^2} + \sigma \frac{\partial \mathbf{E}}{\partial t}$$

From the previous equation we can then write

$$\nabla \times \left(\frac{1}{\mu} \nabla \times \mathbf{E} \right) = -\epsilon \frac{\partial^2 \mathbf{E}}{\partial t^2} - \sigma \frac{\partial \mathbf{E}}{\partial t}$$

Expanding the first term, multiplying through by μ and noting that

$$\mu \nabla \left(\frac{1}{\mu} \right) = -\nabla \ln \mu$$

we get

$$\nabla \times \nabla \times \mathbf{E} + \epsilon\mu \frac{\partial^2 \mathbf{E}}{\partial t^2} + \sigma\mu \frac{\partial \mathbf{E}}{\partial t} = (\nabla \ln \mu) \times \nabla \times \mathbf{E}. \quad (A.1)$$

Expanding equation (6) we have

$$\epsilon \nabla \cdot \mathbf{E} + \mathbf{E} \cdot \nabla \epsilon = 0 \quad \text{or} \quad \nabla \cdot \mathbf{E} = -\mathbf{E} \cdot \nabla \ln \epsilon$$

Hence, using the vector identity

$$\nabla \times \nabla \times \mathbf{E} = -\nabla^2 \mathbf{E} + \nabla(\nabla \cdot \mathbf{E})$$

from equation (A.1), we obtain the following wave equation for the electric field

$$\nabla^2 \mathbf{E} - \epsilon\mu \frac{\partial^2 \mathbf{E}}{\partial t^2} - \sigma\mu \frac{\partial \mathbf{E}}{\partial t}$$

$$= -\nabla(\mathbf{E} \cdot \nabla \ln \epsilon) - (\nabla \ln \mu) \times \nabla \times \mathbf{E}$$

This equation is inhomogeneous in ϵ, μ and σ and its solutions provide information on the behaviour of the electric field in an inhomogeneous non-conductive and/or high conduction dielectric environment. In order to derive such a solution, it must be re-cast in the form of a Langevin equation [16]. By adding

$$\epsilon_0 \frac{\partial^2 \mathbf{E}}{\partial t^2} - \frac{1}{\mu_0} \nabla \times \nabla \times \mathbf{E}$$

to both sides of equation (A.1) and re-arranging the result, we can write

$$\nabla \times \nabla \times \mathbf{E} + \epsilon_0\mu_0 \frac{\partial^2 \mathbf{E}}{\partial t^2}$$

$$= -\epsilon_0\mu_0\gamma_\epsilon \frac{\partial^2 \mathbf{E}}{\partial t^2} - \mu_0\sigma \frac{\partial \mathbf{E}}{\partial t} + \nabla \times (\gamma_\mu \nabla \times \mathbf{E})$$

where

$$\gamma_\epsilon = \frac{\epsilon - \epsilon_0}{\epsilon_0} \quad \text{and} \quad \gamma_\mu = \frac{\mu - \mu_0}{\mu}$$

With equation (6), we can then use the result (valid for $\rho \sim 0$)

$$\nabla \times \nabla \times \mathbf{E} = -\nabla^2 \mathbf{E} + \nabla(\nabla \cdot \mathbf{E}) = -\nabla^2 \mathbf{E} - \nabla(\mathbf{E} \cdot \nabla \ln \epsilon)$$

so that the above wave equation can be written as

$$\nabla^2 \mathbf{E} - \epsilon_0\mu_0 \frac{\partial^2 \mathbf{E}}{\partial t^2} = \mu_0\epsilon_0\gamma_\epsilon \frac{\partial^2 \mathbf{E}}{\partial t^2}$$

$$+\mu_0\sigma \frac{\partial \mathbf{E}}{\partial t} - \nabla(\mathbf{E} \cdot \nabla \ln \epsilon) - \nabla \times (\gamma_\mu \nabla \times \mathbf{E})$$

Finally, introducing the Fourier transform

$$\mathbf{E}(\mathbf{r}, t) = \frac{1}{2\pi} \int_{-\infty}^{\infty} \widetilde{\mathbf{E}}(\mathbf{r}, \omega) \exp(i\omega t) d\omega$$

we can write the above wave equation in the time independent form

$$(\nabla^2 + k^2)\widetilde{\mathbf{E}} = -k^2\gamma_\epsilon \widetilde{\mathbf{E}} + ikz_0\sigma\widetilde{\mathbf{E}}$$

$$-\nabla(\widetilde{\mathbf{E}} \cdot \nabla \ln \epsilon) - \nabla \times (\gamma_\mu \nabla \times \widetilde{\mathbf{E}}) \quad (A.2)$$

where

$$k = \frac{2\pi}{\lambda} = \frac{\omega}{c_0}, \quad c_0 = \frac{1}{\sqrt{\epsilon_0\mu_0}} \quad \text{and} \quad z_0 = \mu_0 c_0$$

Here, λ is the wavelength and ω is the (angular) frequency of the electric wavefield. The parameter z_0 is the free space wave impedance and is approximately equal to 376.6 Ohms. The constant c_0 is the velocity at which electromagnetic waves propagate in a 'free space'.

Acknowledgments

Jonathan Blackledge is supported by the Science Foundation Ireland Stokes Professorship Programme. Bazar Babajanov is funded by the Erasmus Mundus Programme managed by Warsaw University of Technology. The material given in Section I is based on the Distinguished Lecture by Marta Martnez Vźquez, IMST GmbH, [12]. The material in Section VII which provides a background to Fractal Antennas is based on an edited version of the document *Fractal Antennas* by P. Felber Illinois Institute of Technology, December 12, 2000 [35]. The authors are grateful to the Antenna and High Frequency Research Centre `http://ahfr.dit.ie/` at Dublin Institute of Technology.

References

[1] E. Sulic, B. Pell, S. John, R. Gupta, W. Rowe K. Ghorbani and K. Zhang, *Deformation Evaluation of Embedded Antennas in Vehicular Components*, Proceedings of the World Congress on Engineering 2010 Vol III WCE 2010, June 30 - July 2, 2010, London, UK, 1-6, ISBN: 978-988-18210-8-9; `http://www.iaeng.org/publication/WCE2010/WCE2010_pp2389-2394.pdf`

[2] S. Kamboj, and R. Dahiya, *Adaptive Antenna Array for Satellite Communication Systems*, Proceedings of the International MultiConference of Engineers and Computer Scientists 2008 Vol II, IMECS 2008, 19-21 March, 2008, Hong Kong, 1-4; `http://www.iaeng.org/publication/IMECS2008/IMECS2008_pp1491-1494.pdf`

[3] A. L. Mohammad, A. K. Gharevaise, M. Mashinchi M and S. M. Vaezi-Nejad, *A Novel Algorithm based on Fuzzy Optimization for Antenna Arrays*

used in Radio Mobile Communications, Proceedings of the World Congress on Engineering 2008 Vol III WCE 2008, July 2 - 4, 2008, London, UK, 1-6; http://www.iaeng.org/publication/WCE2008/WCE2008_pp1762-1767.pdf

[4] A. Atmaca, C. Ceken and I. Erturk, *Improving Wireless TDMA/FDD MAC Performance with Multi-beam Directional Antennas*, Proceedings of the World Congress on Engineering and Computer Science 2007, WCECS 2007, October 24-26, 2007, San Francisco, USA, 1-6; http://www.iaeng.org/publication/WCECS2007/WCECS2007_pp353-358.pdf

[5] O. W. Ata and N. A. M. Al-Amleh, *Application of MIMO Smart Antennas into WiMAX-OFDM System in Real Fading IEEE Standardized Channels*, Proceedings of the World Congress on Engineering and Computer Science 2012 Vol II WCECS 2012, October 24-26, 2012, San Francisco, USA, 1-6; http://www.iaeng.org/publication/WCECS2012/WCECS2012_pp960-966.pdf

[6] E. G. Lim, Z. Wang, C. U. Lei, Y. Wang and K. L. Man, *Ultra Wideband Antennas - Past and Present*, IAENG International Journal of Computer Science Vol 37, No. 3, 1-11, 2010; http://www.iaeng.org/IJCS/issues_v37/issue_3/IJCS_37_3_12.pdf

[7] Feko Comprehensive Electromagnetic Solution http://www.feko.info/

[8] Electromagnetic Works http://www.emworks.com/

[9] Computer Simulation Technology, http://www.cst.com/Content/Products/MST/Overview.aspx

[10] , L. J. Chu, *Physical Limitations on Omnidirectional Antennas*, Journal of Applied Physics, Vol. 19, pp 1163-1175, 1948.

[11] R. C. Hansen, *Fundamental Limitations in Antennas*. Proceedings of the IEEE Vol. 69, No. 2, 170182, 1981. http://www.cs.berkeley.edu/~culler/AIIT/papers/radio/Hansen%201981%20Fundamental%20Limitations%20in%20Antennas.pdf

[12] M. M. Vázquez, *Design of antennas for mobile communications devices: practical aspects*, IEEE AP-S Distinguished Lecture August 2011, http://www.ieeeboston.org/publications/society_presentations/2011-9-9_presentations/dl_small_antennas.pdf

[13] S. Cloude, *An Introduction to Electromagnetic Wave Propagation and Antennas*, Springer, 1996.

[14] M. Fujimoto, *Physics of Classical Electromagnetism*, Springer, 2007.

[15] J. M. Blackledge, *Digital Image Processing*, Horwood, 2006.

[16] W. Coffey, Y. P. Kalmykov and J. T. Waldron, *The Langevin Equation: With Applications in Physics, Chemistry, and Electrical Engineering*, World Scientific, 1996.

[17] P. M. Morse and H. Feshbach, *Methods of Theoretical Physics*, McGraw-Hill, 1953

[18] P. A. Martin, *Multiple Scattering: Interaction of Time-Harmonic Waves with N Obstacles*, Encyclopedia of Mathematics and its Applications 107, Cambridge University Press, 2006.

[19] J. M. Blackledge, T. Hamalainen and J. Joutsensalo, *Inverse Scattering Solutions with Applications to Electromagnetic Signal Processing*, ISAST Transactions on Electronics and Signal Processing Vol. 4, No 1, 43-60, 2009.

[20] J. M. Blackledge, *Inverse Schrodinger Scattering for Low Gradient Fields*, ISAST Transactions On Computers and Intelligent Sys- tems, Vol. 3, No. 1, 10-23, 2011.

[21] R. A. Shelby, D. R. Smith and S. Shultz, *Experimental Verification of a Negative Index of Refraction.* Science 292 (5514): 7779, 2001.

[22] , N. Cohen, *Fractal Antenna Applications in Wireless Telecommunications*, IEEE Electronics Industries Forum of New England, 43-49, 1997.

[23] Fractal Antenna Systems Inc. http://www.fractenna.com/

[24] C. P. Baliarda, J. Romeu, R. Pous and A. Cardama, *On the Behavior of the Sierpinski Multi-band Fractal Antenna*, IEEE Transactions on Antennas and Propagation, Vol. 46, No. 4, 517-524, April 1998.

[25] C. P. Baliarda, J. Romeu and A. Cardama, *The Koch Monopole: A Small Fractal Antenna*. IEEE Transactions on Antennas and Propagation, Vol. 48, No. 11, 17331781, 2000.

[26] Y. Kim and D. L. Jaggard, *The Fractal Random Array*, Proc. IEEE, Vol. 74, No. 9, 1278-1280, 1986.

[27] A. Shlavinski, E. Heyman and R. Kastner, *Antenna Characterization in the Time Domain*, IEEE Transactions on Antennas and Propagation Vol. 45, No. 7, 1140=1149, 1997.

[28] Time Analysis of UWB Antennas, http://www.feko.info/applications/white-papers/time-analysis-of-UWB-antenna/uwb-monopole-antenna

[29] J. M. Blackledge and B. Babajanov, *Near-field Radiation Patterns for an Ultra-Wide-Band Antenna*, ISSC2013, 1-7, 2013 Near-fieldRadiationPatternsforanUltra-Wide-BandAntenna.

[30] Voxelogic, http://www.voxelogic.com

[31] Voxel Sculpturing http://3d-coat.com/voxel-sculpting/

[32] VoxCad, http://www.voxcad.com/

[33] Pendix, http://home.arcor.de/sercan-san/homepage/sangames/sites/project_pendix.html

[34] Pendix Sketch Based 3D modeling http://www.youtube.com/watch?v=LTU9PbEQ-l4

[35] P. Felber, *Fractal Antennas: A Literature Study as a Project for ECE 576*, Illinois Institute of Technology. December 12, 2000. (Revised: January 16, 2001), http://www.ece.iit.edu/~pfelber/fractalantennas.pdf.